Supporting information

Chemo-photothermal effects of doxorubicin/silica-carbon hollow spheres on liver cancer

Ying-Chi Chen[a], Wen-Tai Chiu[a,b,*], Chin Chang[c], Ping-Ching Wu[a,b,e], Ting-Yuan Tu[a,b,d], Hong-Ping Lin[c,d,*] and Hsien-Chang Chang[a,b,d,*]

[a] *Department of Biomedical Engineering, National Cheng Kung University, Tainan, Taiwan*

[b] *Medical Device Innovation Center, National Cheng Kung University, Tainan, Taiwan*

[c] *Department of Chemistry, National Cheng Kung University, Tainan, Taiwan*

[d] *Center for Micro/Nano Science and Technology Research, National Cheng Kung University, Tainan, Taiwan*

[e] *Institute of Oral Medicine, National Cheng Kung University, Tainan, Taiwan*

* Corresponding authors:

hcchang@mail.ncku.edu.tw (HCC), hplin@mail.ncku.edu.tw (HPL), wtchiu@mail.ncku.edu.tw (WTC)

E-mail: hcchang@mail.ncku.edu.tw

Department of Biomedical Engineering, National Cheng Kung University

Address: No.1, Ta-Hsueh Road, Tainan 70101, Taiwan (R.O.C.)

Tel.: +886-6-2757575 ext 63426

FAX: +886-6-2343270

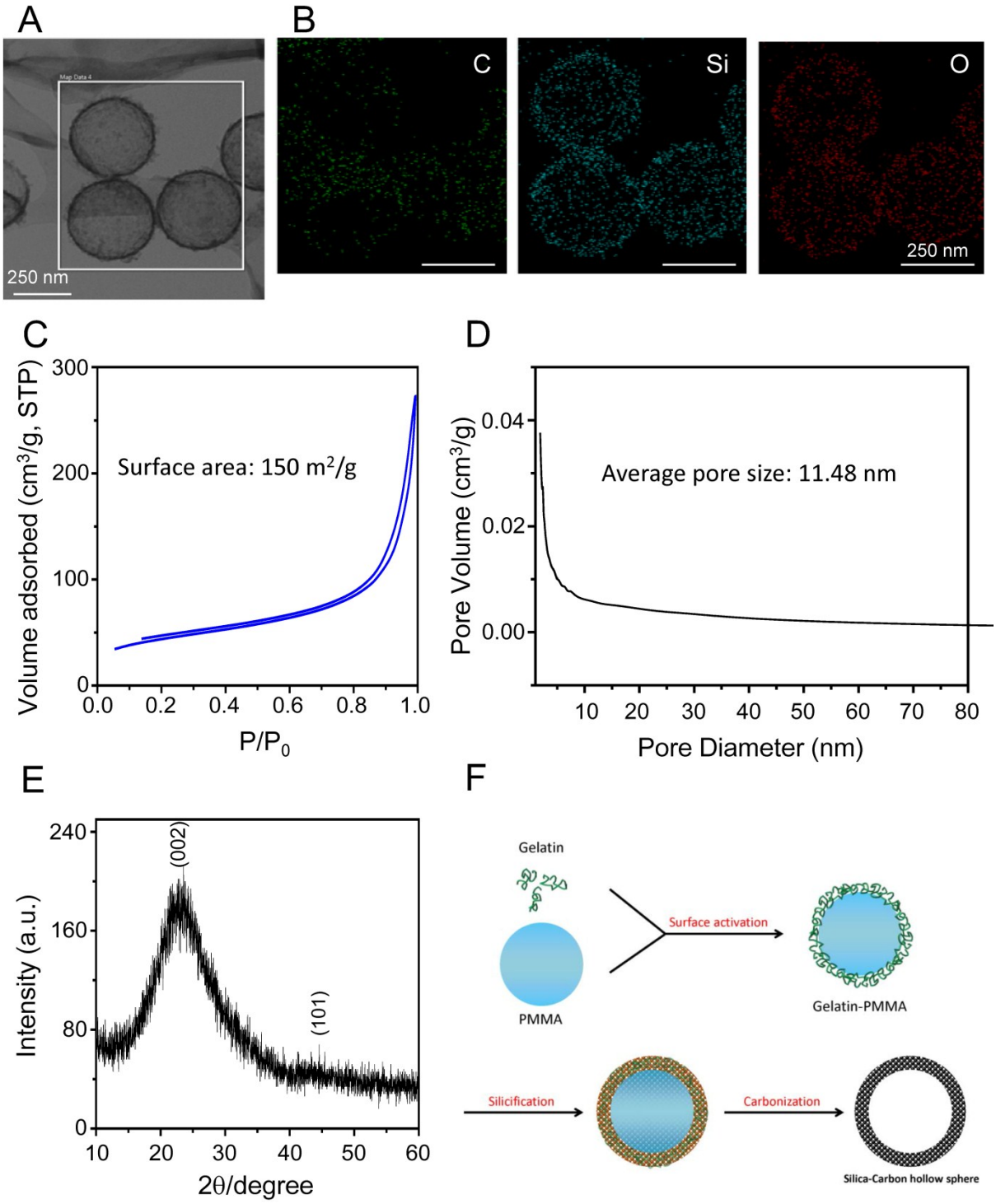

Figure S1. Composition, surface area, and manufacturing processes for SCHSs. (A) TEM image of SCHSs. Scale bar is 250 nm. (B) Elemental mapping of carbon (C), silicon (Si) and oxygen (O) content of SCHSs in the rectangle area in (A) by scanning TEM. (C) The N_2 adsorption-desorption isotherm of SCHSs. (D) Barrett-Joyner-Halenda (BJH) pore-size distribution plot of SCHSs. (E) X-ray diffraction patterns of SCHSs. (F) The proposed mechanism of formation of mesoporous SCHSs.

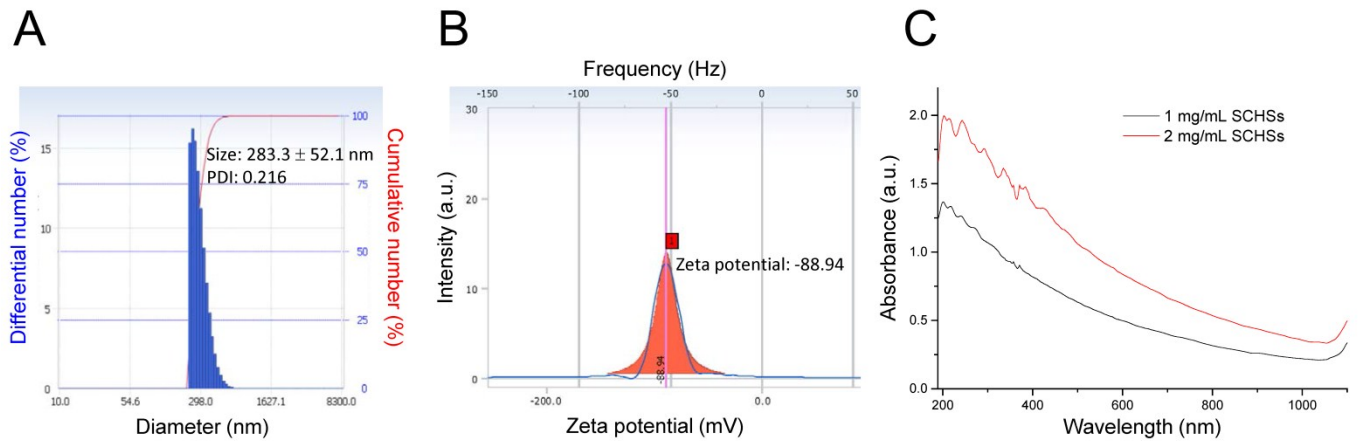

Figure S2. Size, zeta potential and optical properties of SCHSs in solution. (A) Size distribution profile and (B) zeta potential of SCHSs in aqueous solution, measured via dynamic light scattering (DLS). (C) UV-Vis-NIR absorption spectra of SCHSs in distilled water at the concentration of 1 mg/mL and 2 mg/mL.

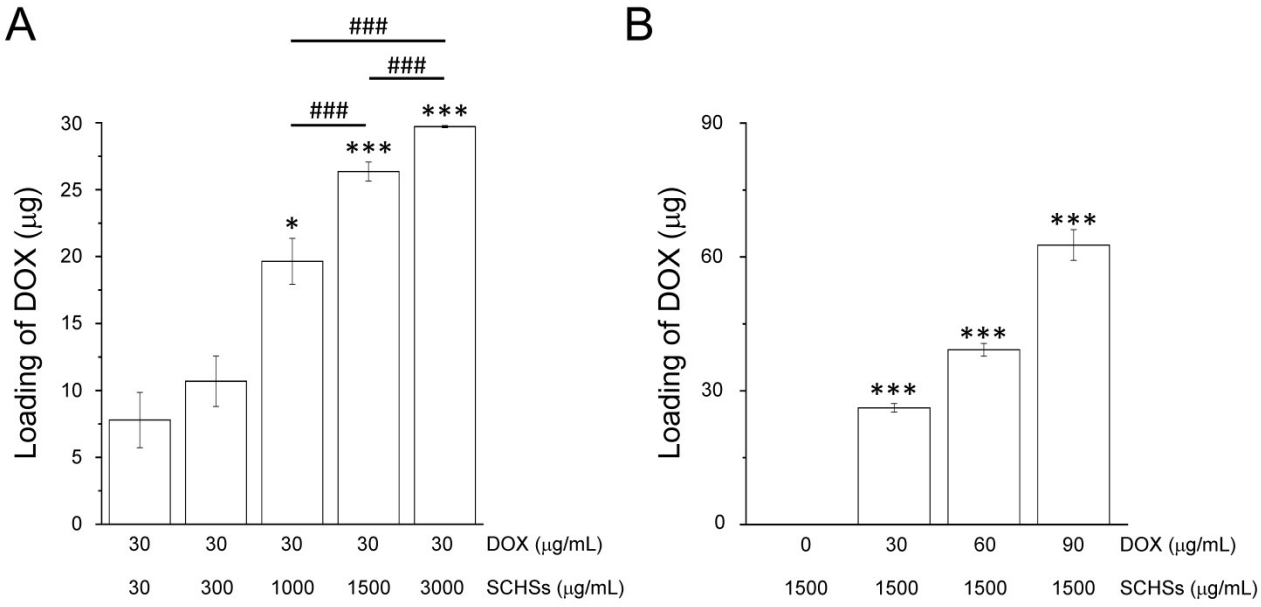

Figure S3. Optimizing components of DOX-SCHSs for DOX loading. A fluorescence microplate reader was used to detect the fluorescent intensity of DOX. Vertical axes represent the mass of DOX for (A) different concentrations (30-3000 μg/mL) of SCHSs mixed with 30 μg/mL DOX and (B) 1500 μg/mL SCHSs mixed with different concentrations of DOX (30-90 μg/mL).

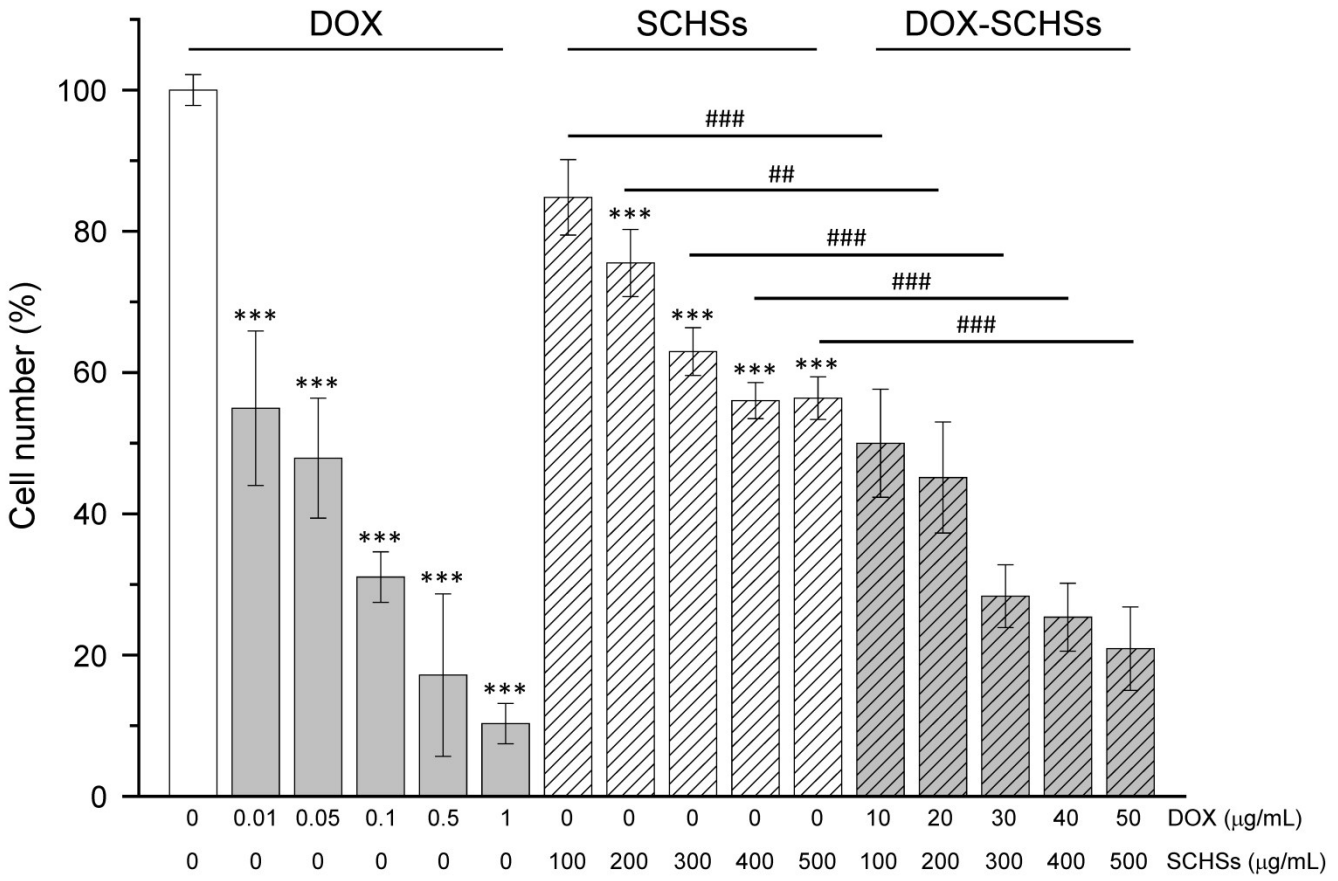

Figure S4. Effects of DOX, SCHSs, and DOX-SCHSs on cell number *in vitro*. ML-1 cells were incubated with DOX, SCHSs, and DOX-SCHSs at different concentrations for 24 h. Hoechst 33342-stained cells were analyzed via fluorescence microscopy to calculate the cell numbers. Each column represents the mean ± SEM from at least three independent experiments. Data were found to be significant at $p < 0.01$ (indicated by ##) or $p < 0.001$ (indicated by ***, ###).

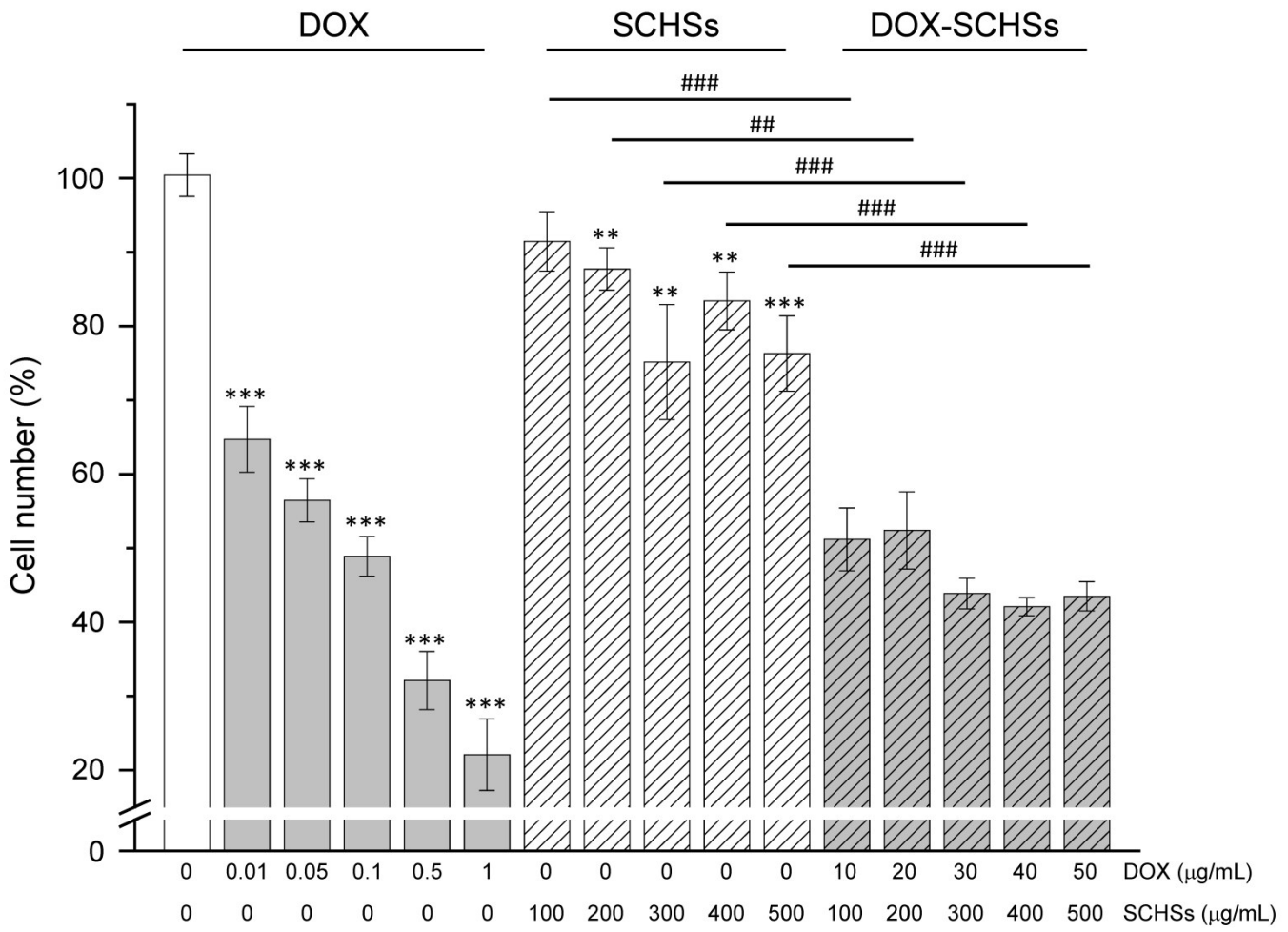

Figure S5. Effects of DOX, SCHSs, and DOX-SCHSs on cell number *in vitro*. Huh-7 cells were incubated with DOX, SCHSs, and DOX-SCHSs at different concentrations for 24 h. Hoechst 33342-stained cells were analyzed via fluorescence microscopy to calculate cell numbers. Each column represents the mean ± SEM of at least three independent experiments. Data were considered to be statistically significant at $p < 0.01$ (indicated by **, ##) or $p < 0.001$ (indicated by ***, ###).

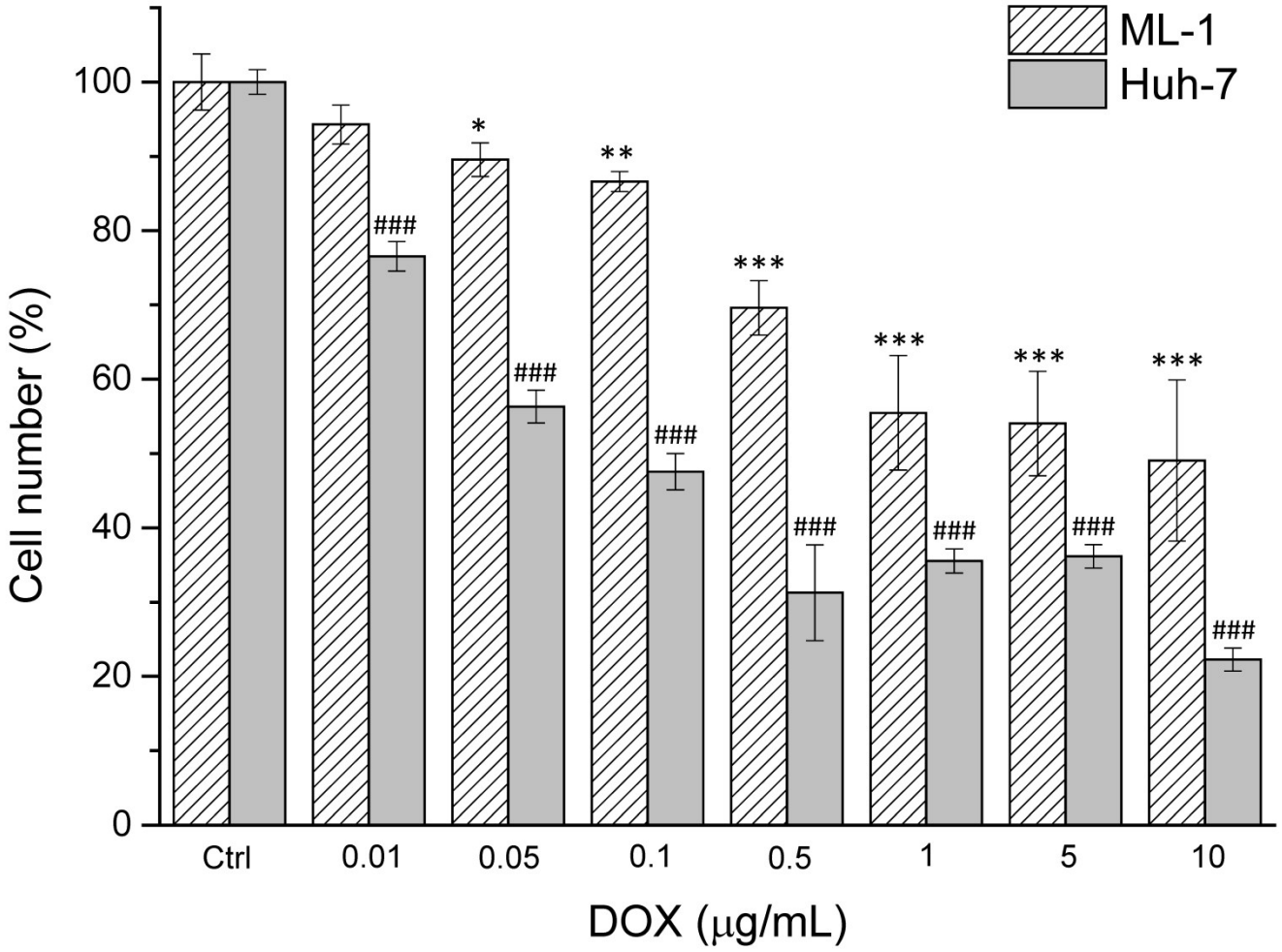

Figure S6. Effects of DOX on cell number in monolayer cell culture *in vitro*. Monolayers of hepatoma cells were incubated with DOX at different concentrations for 24 h. Hoechst 33342-stained cells were analyzed via fluorescence microscopy to calculate the cell numbers. Each column represents the mean ± SEM from at least three independent experiments. Data were found to be significant at $p < 0.05$ (indicated by *), $p < 0.01$ (indicated by **), or $p < 0.001$ (indicated by ***, ###).

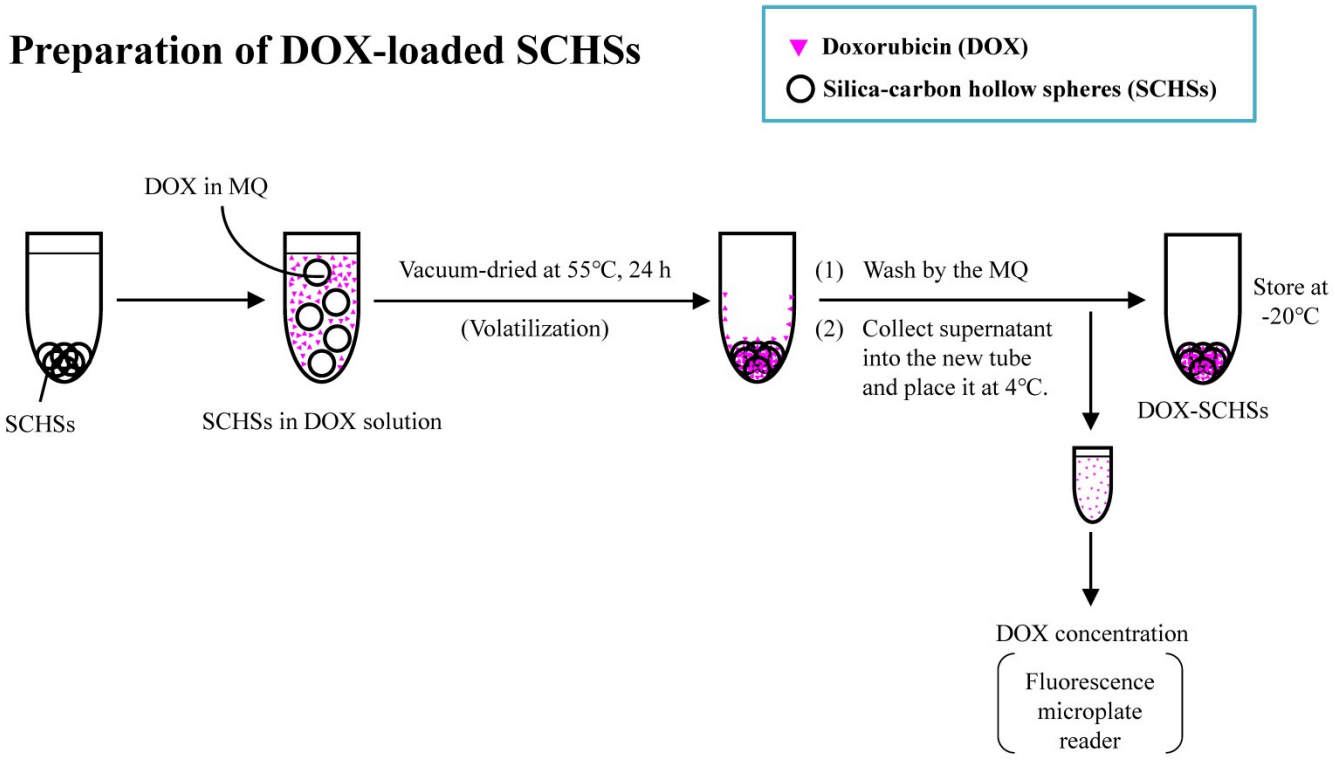

Figure S7. The process of preparation of DOX-loaded SCHSs.